Optical emission of a plasma from low-density targets irradiated with coherence-controllable laser radiation*

A.A. Fronya, N.G. Borisenko, V.N. Puzyrev, A.T. Sahakyan, A.N. Starodub, O.F. Yakushev

Abstract. **The results of experiments on the interaction of nanosecond laser radiation with low-density volume-structured targets of different density and thickness are reported. The targets were irradiated by laser radiation with controllable coherence. The primary objective was to investigate the effect of target parameters on the characteristics of radiation scattered by the plasma. The spectral characteristics of the radiation scattered by the plasma in the backward direction and in the direction of laser beam propagation were obtained. Also the radiation scattering patterns were recorded.**

Keywords: laser-produced plasma, plasma-scattered radiation, interaction of laser radiation with matter.

1. Introduction

One of the central problems in the interaction of high-power laser radiation with matter is the efficiency of laser energy transfer to the plasma. The scattering that occurs in the plasma has a significant effect on the absorption of laser radiation by the plasma. It is therefore critically important to comprehensively investigate the scattering in laser-produced plasmas, specifically, to study the spectral, temporal, spatial and energy characteristics of the scattering.

Another important problem that has to be solved is to provide a uniform distribution of laser energy over the surface of the target under irradiation, which also affects the efficiency of laser-to-target energy transfer. To this end, Voronich et al. [1] proposed the method of a dynamic plasma phase plate implying optical transparency of the plasma layer, which is possible with the use of low-density microstructured objects.

Experiments in the interaction of laser radiation with low-density targets are performed in many laboratories in the world [2–6]. Several papers [7–10] are concerned with the study of shock waves in the plasma produced when low-density targets of different structure are irradiated by high-intensity beams. In the investigation of shock wave propagation through the plasma, the changes in wavefront propagation are recorded from the intrinsic X-ray and optical plasma radiation. For instance, for a heating radiation wavelength $\lambda_0 = 527$ nm, Koenig et al. [10] observed a thermal plasma glow in a broad optical spectral range (400–800 nm) with two well pronounced maxima in the vicinity of $\lambda = 450$ and 700 nm.

Investigations of the radiation scattered by the plasma encompass the study of processes like stimulated Raman scattering (SRS), stimulated Brillouin scattering (SBS) and harmonic generation in the plasma. For instance, Dunne et al. [11] discovered that less than 5% of the incident laser energy is converted to the SBS component for layered targets and less than 3% for flat solid films of C_8H_8 (these measurements were performed within the aperture of the focusing optics). The authors noted that the spectral characteristics of the SRS and SBS were hardly changed when the system of laser radiation focusing was modified. The temporal evolution of the second harmonic of laser radiation (for a wavelength $\lambda_0 = 1.054$ μm and a pulse duration of 3 ns) was studied in Ref. [12]. For targets with a quasi-ordered structure the second harmonic generation was found to occur periodically during the course of the laser pulse.

In the study of laser beam 'smoothing' on the LIL facility (for a laser energy of 10 kJ and a pulse duration of 2.7 ns at a wavelength of 351 nm) [3], it was determined that the foam with a density of 10 mg cm^{-3} and a thickness of 500 μm is completely ionised in 1.2 ns. Temporally resolved SBS measurements for a compound target (a foam layer of thickness 500 μm on a Cu substrate) revealed the existence of two components separated in time by 1.2 ns. They corresponded to the SBS in the foam (the earlier component) and the SBS in the Cu substrate for a completely ionised foam. The SBS from the foam exhibits a red shift. The effect of laser beam smoothing after transmission through the foam was demonstrated.

In Ref. [2] it was discovered that the laser energy fraction transmitted through triacetate cellulose (TAC) targets may be as high as 50%. In this case, the reflected energy fraction was equal to ~12%. A plasma afterglow was observed after the termination of laser pulse irradiation. The plasma was found to be transparent for the rise-up portion of the heating radiation pulse (for a laser pulse duration of ~0.34 ns).

However, in experiments with agar-agar targets, the energy fraction transmitted through the target was equal to ~2% [13]. The plasma transmittance rose towards the end of the heating radiation pulse. The temporal behaviour of the radiation at the frequencies $2\omega_0$ and $(3/2)\omega_0$ was studied (ω_0 is the heating radiation frequency): the plasma glows through-

A.A. Fronya P.N. Lebedev Physics Institute, Russian Academy of Sciences, Leninsky prosp. 53, 119991 Moscow, Russia; National Research Nuclear University 'MEPhI', Kashirskoe sh. 31, 115409 Moscow, Russia; e-mail: nastya708@yandex.ru;
N.G. Borisenko, V.N. Puzyrev, A.T. Sahakyan, A.N. Starodub, O.F. Yakushev P.N. Lebedev Physics Institute, Russian Academy of Sciences, Leninsky prosp. 53, 119991 Moscow, Russia

out the time of irradiation by the heating radiation. The spectra of both harmonics exhibit a two-component structure; clearly pronounced in the second harmonic case is an asymmetry of the spectrum.

In the present work we outline the results of a series of scattering experiments in the plasma produced by irradiating low-density microstructured TAC targets by the laser radiation with controllable coherence.

2. Experimental conditions

The experiments in the interaction of laser radiation with targets were performed on the Kanal-2 facility [14]. The laser radiation parameters were as follows: a half-amplitude duration of 2.5 ns, a half-height spectral radiation width of 24 Å or 42 Å, an output laser energy of $1-100$ J, and a heating radiation intensity of $10^{12}-10^{14}$ W cm^{-2} at the target.

The diagnostic complex employed in these experiments comprised:

– a spectrograph-based channel intended for investigating the spectral characteristics of plasma radiation in the $0.4-1.1$ μm range;

– an optical system which permits obtaining information about the directions of plasma expansion and laser radiation scattering at a given section in an angular detection range $\Delta\alpha \approx 90°$ and in a spectral range $\Delta\lambda \approx 0.4-1.1$ μm; and

– a calorimetric system intended for measuring the energy characteristics of plasma and laser radiation.

3. Experimental results and their discussion

Low-density microstructured objects, which were three-dimensional polymer TAC meshes [15], were employed as irradiation objects. In these experiments, the density of TAC targets was varied from 2 to 10 mg cm^{-3} and their thickness from 100 to 500 μm. The distance between the fibres ranged from 0.6 to 1.7 μm and the fibre diameter ranged from 70 to 40 nm. In some cases, the target incorporated copper nanoparticles with an average diameter of 40 nm. The laser radiation was normally incident on the target surface in all experiments. For the $\lambda_0 = 1.054$ μm wavelength of laser radiation the critical density is equal to ~3 mg cm^{-3} (for a single ionisation of atoms). The bulk critical density of the target was estimated using formula (1.109) from Ref. [16]. Therefore, our experiments studied the radiation interaction with TAC targets with critical as well as subcritical bulk densities.

Previous data on the penetration of high-intensity laser radiation through low-density TAC targets showed that the energy fraction transmitted through these targets might be as high as 70% of the incident laser energy [6]. At the same time, the reflected energy fraction does not exceed 1% of the incident laser energy. In this case, the energy fraction transmitted through the target becomes lower with increasing the density, thickness, and linear mass of the target.

The linear mass of TAC targets was found to affect the angle of radiation scattering [6]. Specifically, the angle of backscattering at the fundamental frequency increases with linear mass. By comparing the fundamental radiation scattering patterns for TAC and solid targets it was determined that they behaved in a similar manner (Fig. 1). In comparison with the patterns obtained using calorimeters for agar-agar targets in Ref. [13], the TAC targets are characterised by a broader scattering pattern. In the case scattering in the incident beam direction behind the plasma of TAC targets, we found that

the radiation scattering patterns for the fundamental and the second harmonic were different. Specifically, the scattering at the second harmonic frequency is diffuse, while the scattering of the fundamental is confined in a finite solid angle whose angular aperture coincides with that of the incident beam (Fig. 2). In this case, the intensity measurement uncertainty does not exceed 2%.
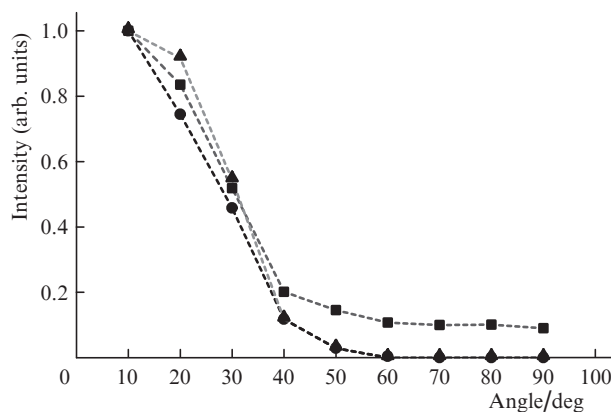
Figure 1. Fundamental radiation backscattering patterns for targets of TAC (10 mg cm^{-3}, 200 μm) (■), Fe (●), and Be (▲).
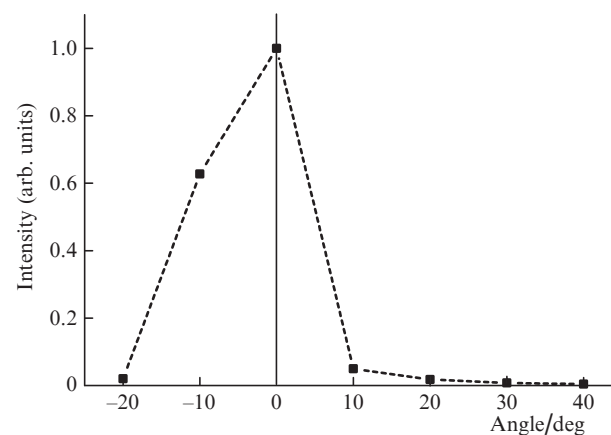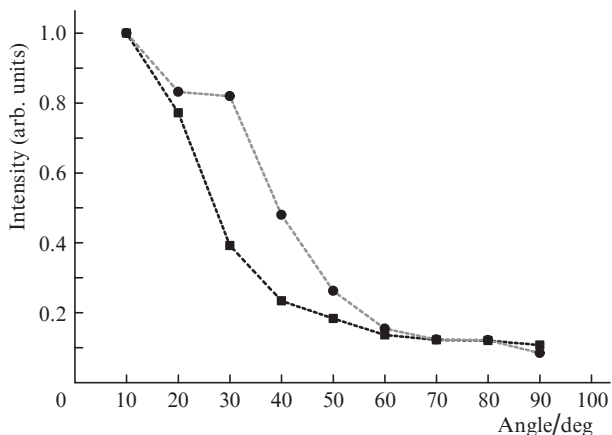

Figure 2. Pattern of fundamental radiation scattering behind the plasma of a TAC target (10 mg cm^{-3}, 200 μm) with an addition of copper. The zero angle corresponds to the direction of heating radiation propagation.

For the TAC targets with additions of copper nanoparticles (which substituted for 10% of polymer mass in the target), the backscattering pattern is different in comparison with the patterns obtained for nanoparticle-free TAC targets. The fundamental radiation scattering patterns show a decrease in intensity with increase in the scattering angle (Fig. 3).

The radiation scattering pattern for the TAC targets with additions of copper depends on what part of the nanoparticles fall within the focal spot of the heating radiation and on how these nanoparticles are distributed in the target. The nanoparticles do not possess a regular spherical shape and it is hard to determine the angle at which the laser radiation is incident on them.
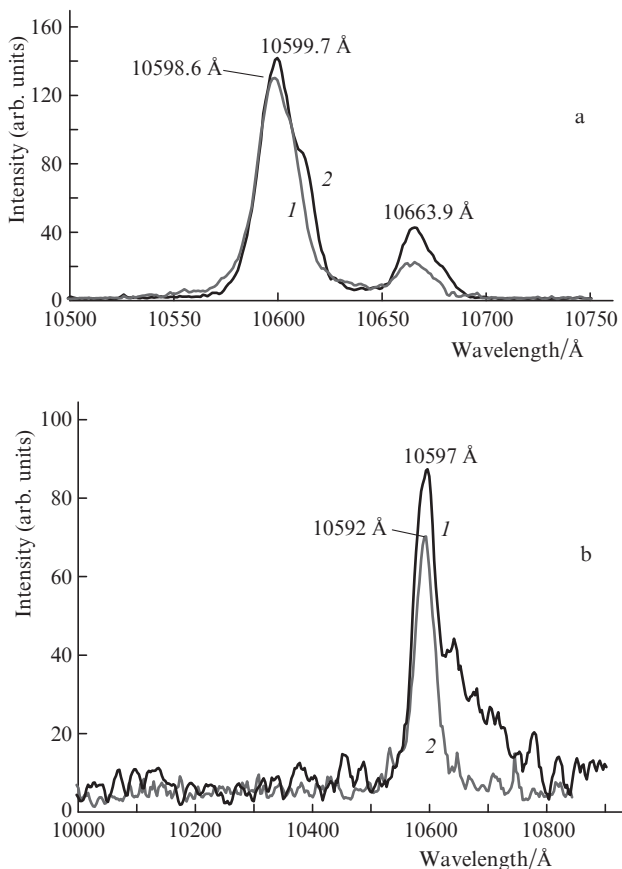
In our experiments, the spectra of radiation scattered by the plasma in the forward and backward directions relative to

Figure 3. Fundamental radiation backscattering patterns for TAC targets (10 mg cm^{-3}, 200 μm) without (■) and with (●) an addition of Cu nanoparticles.

the direction of laser radiation propagation were recorded near the frequencies ω_0 and $2\omega_0$.
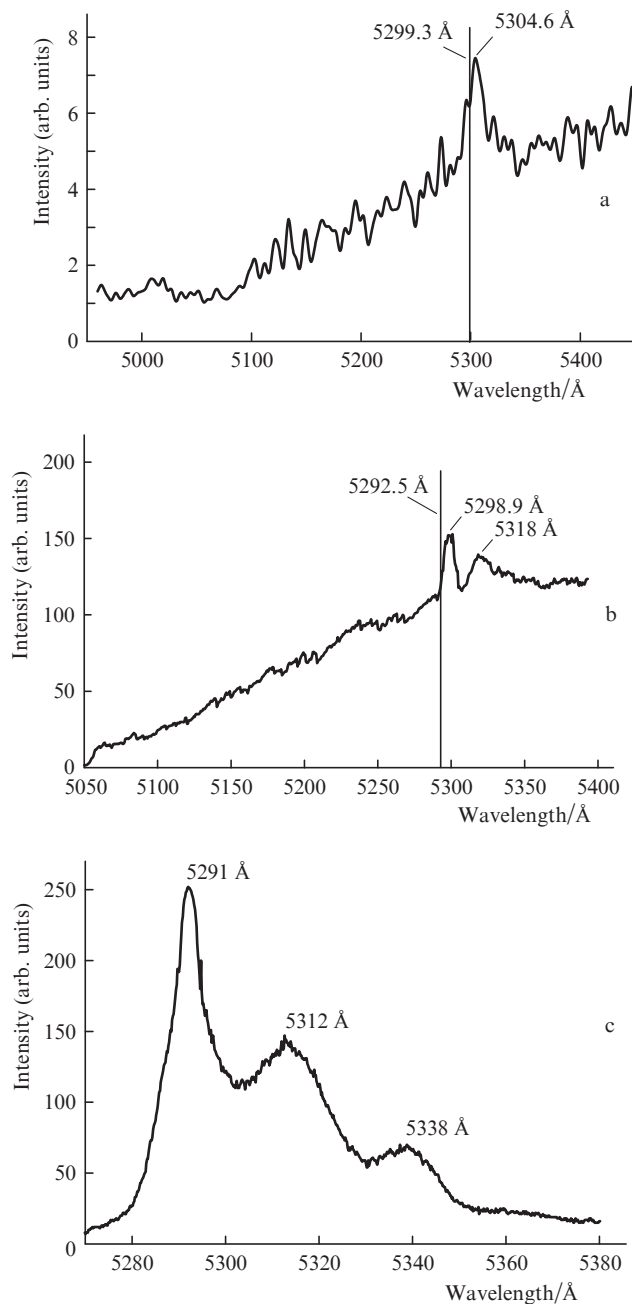
Special emphasis was placed on the fundamental radiation spectra behind the TAC target. We observed changes in the position of the peak of this spectrum relative to the ω_0 frequency as well as in the linewidth of the radiation scattered

near the fundamental frequency. In some experiments the spectral width of the radiation transmitted through the plasma of TAC targets became substantially larger when the spectral width of the heating laser radiation was equal to 42 Å [6]; furthermore, the broadening was inherently asymmetric. Figure 4 depicts the spectral distribution of the fundamental radiation scattered by the plasma in forward direction.

In the spectrum of forward-scattered radiation near the second harmonic frequency $2\omega_0$ there is a low-intensity peak against the continuous background (Fig. 5). The position of this peak relative to $\lambda_0/2$ changed from shot to shot: the peak

Figure 4. Forward-scattered radiation spectra at the fundamental frequency (1) for a TAC target (9 mg cm^{-3}, 400 μm), an energy of the heating radiation of 40.2 J and its spectral linewidth of 24 Å (a), as well as for a TAC target (9 mg cm^{-3}, 200 μm), an energy of 27.5 J and a spectral linewidth of 42 Å (b). Curve (2) stands for the heating radiation spectrum.

Figure 5. Radiation spectra at the second harmonic frequency: forward-scattered radiation, TAC target (4.5 mg cm^{-3}, 400 μm), an energy of the heating radiation of 34.6 J (a); backscattered radiation, TAC target (9 mg cm^{-3}, 400 μm), an energy of 17.8 J (b); backscattered radiation, copper target, an energy of 42.6 J (c). The spectral linewidth of the heating laser radiation is equal to 21 Å.

shifted to the red as well as to the blue side of the spectrum. The displacement of the second harmonic peak to the blue or red domain is indication that the critical density domain is moving either in the opposite direction to the beam or in the direction of its propagation. The second harmonic radiation was recorded on the axis of the heating beam.

The radiation backscattered at a wavelength of $\lambda_0/2$ is characterised by the existence of two peaks against a continuous background, which are nearly always shifted to the red side relative to $\lambda_0/2$ (Fig. 5b). In this case, the spectral broadening is inherently asymmetric.

This structure in the second harmonic spectrum exists due to the processes of two types responsible for the generation of this harmonic: the linear conversion of laser radiation and the development of parametric instabilities. The peak near the $\lambda_0/2$ wavelength arises from the linear conversion of the heating radiation and the pedestal arises from the development of parametric plasma instabilities in the near-critical electron-density region: $n \approx n_c$. The dimension of the domain of plasma glow at the second harmonic frequency corresponds to the focal spot size.

In order for the parametric instabilities to arise, the intensity of laser radiation must exceed a certain critical value. This threshold was estimated using formula (24) in the case of parametric decay and using formula (25) from Ref. [17] in the case of aperiodic instability. For the experimental conditions under consideration, the parametric decay threshold amounted to $\sim 10^{12}$ W cm^{-2} and the aperiodic instability threshold amounted to about 4.5×10^{14} W cm^{-2}. In the investigation of the spectral composition of the radiation scattered by the plasma, the on-target intensity did not exceed $\sim 10^{14}$ W cm^{-2}; in this case, the pedestal and the second peak are present in the second harmonic spectrum. As noted above, the scattering at the second harmonic frequency is diffuse. The spectral shape and the radiation pattern of second harmonic radiation from the plasma of TAC targets suggest that the second harmonic is generated both due to linear conversion and to parametric decay.

It is pertinent to note that harmonics at the frequencies $\omega_0/2$, $(3/2)\omega_0$ and $(5/2)\omega_0$ were recorded in the plasma radiation spectrum with the use of a four-frequency polarisation microscope [18]. This fact also testifies to the development of parametric instabilities in the plasma in the domain with an electron density $n \approx n_c/4$.

Experimental data on the second harmonic generation in low-density target plasmas show that multicomponent structures in second harmonic spectra are characteristic for different spectral widths of laser radiation. Furthermore, such a multicomponent structure was also recorded for a solid copper target (Fig. 5c). The observed spatial distributions of the radiation intensity at the second harmonic frequency are different: for the solid target this distribution is smooth, while the foam is characterised by a nonuniform distribution.

The asymmetric shape of the second harmonic spectrum of the backscattered radiation was discovered for agar-agar targets in Ref. [13]. In this case, the second harmonic was generated even when the average electron density corresponding to complete ionisation of the target substance was lower than the critical density for the 1.054 μm heating radiation.

The resultant experimental data about the present of second harmonic radiation in the scattering spectrum of the plasma testify to the formation of regions with a critical electron density even in targets with a lower bulk density than the calculated critical density for our experimental conditions (below 3 mg cm^{-3}).

From the spectral shift of the second harmonic radiation backscattered by the TAC target plasma, we estimated the velocity of the critical density domain using formula (3) from Ref. [17]:

$$\Delta\omega_2 = 4\omega_0 u/c, \tag{1}$$

where $\Delta\omega_2$ is the second harmonic shift relative to the $2\omega_0$ frequency; u is the velocity of the domain with the critical electron density; and c is the velocity of light. The closest-to-$\lambda_0/2$ peak in the second harmonic spectrum was assumed to result from the linear conversion of the heating radiation in the plasma. For the spectral distribution of the second harmonic depicted in Fig. 5b, the velocity u is equal to $\sim 6 \times 10^6$ cm s^{-1}. In the majority of experiments, the peak of second harmonic spectrum is shifted to the red side relative to $\lambda_0/2$, which corresponds to the motion of the critical density region in the direction of laser beam propagation. However, in some experiments we recorded a blue shift, which is indication that this region moves in the opposite direction to the laser beam.

The second harmonic radiation was recorded integrally throughout the period of laser irradiation and resultant plasma; in this case, the spectral linewidth of second harmonic radiation (of the peak corresponding to the linear conversion) turned out to be smaller than the spectral linewidth $\delta\omega_0$ of the pump radiation. Proceeding from formula (4) from Ref. [17] for the width of second harmonic spectrum

$$\delta\omega_2 = 2\delta\omega_0 + 4\omega_0\delta u/c \tag{2}$$

it is possible to estimate the velocity variations δu of the motion of the critical density region. For an experimentally recorded spectral width of the second harmonic ~ 7 Å, the velocity variation of critical region motion is estimated, according to formula (2), at $\sim 5.6 \times 10^6$ cm s^{-1}.

With increasing intensity of incident radiation, the wavelength shift of second harmonic radiation relative to the wavelength of laser radiation becomes larger, which is supposedly due to the increase in the energy deposited into the plasma and, consequently, to the growth of plasma expansion velocity [17].

Since the target is made up of chaotically arranged fibres and has a density of ~ 300 mg cm^{-3}, laser irradiation with an intensity of $10^{12} - 10^{14}$ W cm^{-2} results in plasma production and, consequently, gives rise to critical density domains. However, a continuous domain with a critical electron density equal in size to the focal spot does not emerge in this material. As is well known, the dimensions of TAC fibres are such that the focal spot covers a target area which contains a huge number of fibres.

The number of fibres accounted for by the focal spot area may be estimated by formula (3) from Ref. [19]:

$$n_p S = \frac{\rho_a}{\pi b_0^2 l_0 \rho_s} S, \tag{3}$$

where n_p is the density of cylindrical particles in the volume of a porous material; S is the area of the material; ρ_a is the average porous material density; ρ_s is the substance density of the solid elements which make up the porous material; b_0 is the radius of a cylindrical element; and l_0 is the length of a cylindrical element. The quantity $n_p S$ amounts to $\sim 10^6$ μm^{-1}.

It is likely that microdomains with a critical density are formed in such a target, these microdomains being randomly distributed over the focal spot area as well as over the target volume. Furthermore, these domains may move in different directions, which gives rise to different shifts of the peaks of the second harmonic spectrum relative to $\lambda_0/2$ in the course of time-integrated spectrum and plasma glow recording.

4. Conclusions

The interaction of laser radiation with low-density TAC targets was experimentally investigated for the purpose of studying the properties of scattering in the laser-produced plasma of such targets.

In the investigation of the spatial distribution of forward-transmitted radiation it was found that the fundamental radiation pattern corresponds to the angular aperture of the incident beam and is independent of target parameters. For the second harmonic radiation the scattering was found to occur diffusely.

Studying the spectral composition of the radiation scattered by the plasma showed that the linewidth of the scattered radiation at the fundamental frequency (both back- and forward-scattered) becomes broader and the positions of the peaks of the spectral distributions near the fundamental ω_0 and the $2\omega_0$ frequency may vary. The spectral broadening of the scattered radiation near the fundamental is due to stimulated processes like SBS and SRS. Observed in some experiments was a significant broadening of the spectrum near the fundamental frequency – up to 200 Å. The second harmonic radiation was recorded for all targets employed in the experiments, which testifies to the formation of critical electron-density domains in the plasma even when the initial target density was subcritical. The plasma scattering data suggest that the second harmonic is generated due to the linear conversion of laser radiation to longitudinal Langmuir oscillations near the domains of critical electron density and the development of parametric plasma instabilities, namely of parametric decay.

References

1. Voronich I.N., Garanin S.G., Dergach V.N., et al. *Quantum Electron.*, **31**, 970 (2001) [*Kvantovaya Elektron.*, **31**, 970 (2001)].
2. Borisenko N.G., Akunets A.A., Khalenkov A.M., et al. *J. Russ. Laser Res.*, **28** (6), 548 (2007).
3. Depierreux S., Labaune C., Michel D.T., et al. *J. Phys.: Conf. Ser.*, **112**, 022041 (2008).
4. Lei A.L., Tanaka K.A., Kodama R., et al. *Phys. Rev. Lett.*, **96**, 255006 (2006).
5. Jung R., Osterholz J., Löwenbrück K., et al. *Phys. Rev. Lett.*, **94**, 195001 (2005).
6. Starodub A.N., Borisenko N.G., Fronya A.A., et al. *Laser Part. Beams*, **28**, 371 (2010).
7. Benuzzi A., Koenig M., Krishnan J., et al. *Phys. Plasmas Lett.*, **5**, 2827 (1998).
8. Dezulian R., Ganova F., Barbanotti S., et al. *Phys. Rev. E*, **73**, 047401 (2006).
9. Drake R.P., Glendinning S.G., Estabrook K., et al. *Phys. Rev. Lett.*, **81**, 2068 (1998).
10. Koenig M., Philippe F., Benuzzi-Mounaix A., et al. *Phys. Plasmas*, **10**, 3026 (2003).
11. Dunne M., Borghesi M., Iwase A., et al. *Phys. Rev. Lett.*, **75**, 3858 (1995).
12. Bugrov A.E., Burdonskii I.N., Gavrilov V.V., et al. *Plasma Phys. Rep.*, **30**, 143 (2004).
13. Bugrov A.E., Burdonskii I.N., Gavrilov V.V., Gol'tsov A.Yu., et al. *Zh. Eksp. Teor. Fiz.*, **115**, 805 (1999).
14. Fedotov S.I., Feoktistov L.P., Osipov M.V., Starodub A.N. *J. Russ. Laser Res.*, **25**, 79 (2004).
15. Borisenko N.G., Akimova I.V., Gromov A.I., et al. *Fusion Sci. Technol.*, **49**, 676 (2006).
16. Afanas'ev Yu.V., Basov N.G., Krokhin O.N., et al. *Itogi Nauki i Tekhniki. Ser. Radiotekhnika. Vol. 17* (Moscow: VINITI, 1978).
17. Basov N.G., Bychenkov V.Yu., Krokhin O.N., et al. *Sov. J. Quantum Electron.*, **9**, 1081 (1979) [*Kvantovaya Elektron.*, **6**, 1829 (1979)].
18. Vasin B.L., Mal'kova S.V., Osipov M.V., et al. *Prikl. Fiz.*, **6**, 152 (2009).
19. Gus'kov S.Yu., Rozanov V.B. *Quantum Electron.*, **27**, 696 (1997) [*Kvantovaya Elektron.*, **24**, 715 (1997)].